6

Adventures with Smart Chemical Sensing

Electrooptically Responsive Photonic Crystals

Sanford A. Asher
Department of Chemistry
University of Pittsburgh

6.1 INTRODUCTION

There is intense interest in the development of photonic crystal materials for applications in optics, optical computing and for the control of electromagnetic radiation propagation.[1-3] The excitement in this area stems from the recent development of a deep understanding of light propagation within materials with periodic optical dielectric constant modulations, and the development of fabrication methods for forming these materials.[4]

The synthetic and fabrication communities have been challenged to develop photonic crystals with the appropriate crystal structures and the dielectric constant modulations that enable the photonic crystals to possess three-dimensional photonic bandgaps in the visible and near IR spectral regions.[5] Electromagnetic radiation within a bandgap would be unable to propagate in a 3-D photonic bandgap material at any angle; thus, unique phenomena would occur; for example, spontaneous emission would disappear. Any light in the bandgap that entered the 3-D photonic bandgap material, through a purposely fabricated defect structure, could be made to traverse tortuous paths, such as, for example, 90 ° bends, without significant intensity losses. These possibilities enable a number of fantasies, such as fabricating complex photonic chips made out of 3-D photonic bandgap

materials that contain numerous optical transistors and switching devices, all made from photonic crystals.

As discussed below, the future appears bright for the development of photonic crystals for the control of light propagation. The rate limiting step is the development of methods to fabricate appropriate materials to test recent theories for propagation and control of light in photonic materials.

The first fabrication methods for forming photonic crystals utilized crystalline colloidal self assembly.[6] In this approach highly charged monodisperse spherical colloidal particles were dispersed in pure water.

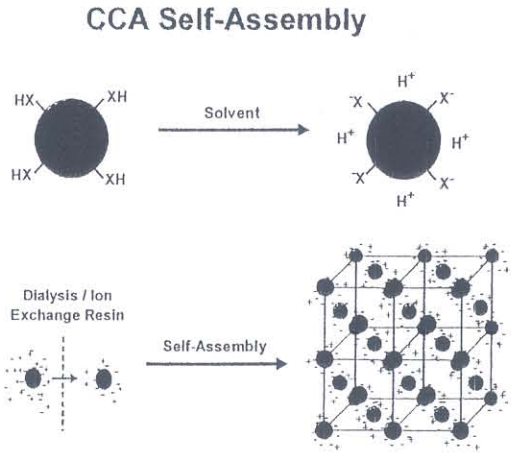

FIGURE 6.1. A dispersion of monodisperse colloidal particles with strong acid groups on their surfaces self assemble into fcc or bcc crystalline colloidal arrays in low ionic strength solution. Ions can be removed from colloidal dispersions by techniques such as dialysis, for example.

These spheres were functionalized with thousands of strong acid groups which ionized in water to result in a high surface charge (Figure 6.1). Because these highly charged spheres repel each other over macroscopic distances (Figure 6.2), the system finds a well defined minimum energy state. This minimum energy state involves the self assembly of these particles into an fcc lattice (a bcc structure is also observed under some conditions).

Monodisperse colloidal particles were first synthesized in the 1950's by Alfrey et al[7], a group from Dow Chemical. It was immediately obvious from TEM studies that these monodisperse polystyrene spherical particles easily formed highly ordered close packed arrays when aqueous dispersions of them were dried on TEM grids. Hiltner and Krieger[7,8] were among the first to note that cleaned dispersions of these monodisperse, charged particles would Bragg diffract visible light. The Asher group was the first to demonstrate that this colloidal crystalline array (CCA) self assembly could

be used to form large fcc single crystals, where the fcc (111) planes oriented parallel to the quartz plates which enclosed the crystal[6,9] (Figure 6.3). This enabled fabrication of photonic crystals which used the one dimensional fcc (111) plane band gap for filtering light in the visible spectral region.[6,9]

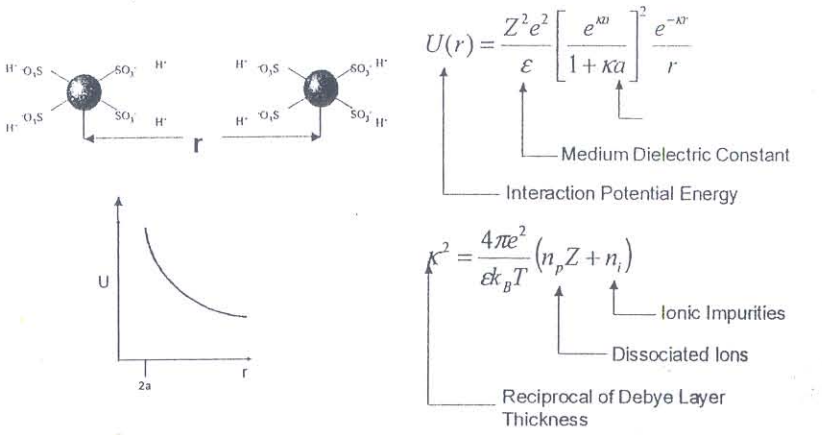

FIGURE 6.2. CCA self assembly results from the electrostatic repulsion between colloidal particles. This interaction is modeled by the DLVO potential as increasing with the square of the colloidal particle charge, and inversely with the solution dielectric constant. It exponentially decreases with the Debye layer length, κ^{-1} which decreases with the solution ionic strength. The repulsion can be significant over macroscopic distances. For example, κ^{-1} is limited to 700 nm in pure water due to the concentrations of the H^+ and OH^-.

The Bragg diffraction efficiency of these CCA were extraordinarily high (Figure 6.3 and 6.4); for example, a thin 400 μm thick CCA of 270 nm diameter polystyrene spheres in water diffract away essentially all 488 nm light from a 1 W Ar laser, and allows brave observers to directly look down a lasing Ar^+ laser plasma tube.[6,9]

EG&G Princeton Applied Research Corp. was the first company to commercialize photonic crystals by manufacturing CCA filters for use in rejecting laser light. This commercialization occurred through their licensing of the first photonic crystal patents[6] from the University of Pittsburgh in the mid 1980's.

The major difficulty with the CCA photonic crystal devices is that they are potentially unstable, if not prepared with very pure materials and with careful attention to the sample container. CCA fabricated under appropriate conditions have shown over ten years of stability.

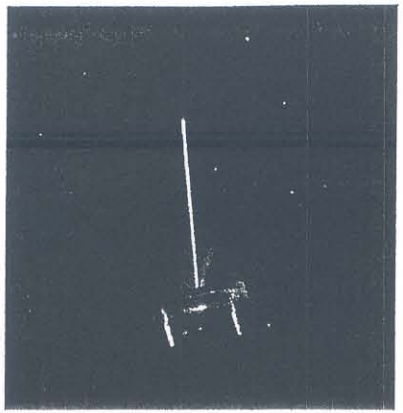

FIGURE 6.3. Diffraction of 488 nm laser light by an fcc CCA whose (111) planes diffract normally incident 1.4 μm light. The liquid CCA of 270 nm diameter spheres shows the diffraction of three beams from higher Miller indice planes. The ~100 μm thick fcc crystal is contained between two quartz plates. The fcc (111) planes spontaneously orient parallel to the quartz plate surfaces.

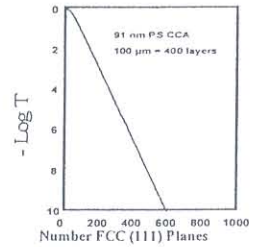

FIGURE 6.4. Calculated transmission through fcc CCA of 91 nm diameter polystyrene spheres in water diffracting 488 nm light. The transmittance is calculated to be less $\sim 10^{-7}$ for 400 (111) planes, which corresponds to a CCA thickness of ~100 μm. Adapted from Spry and Kosan (ref. 13).

The fcc lattice is kinetically stabilized by repulsive interactions. In the absence of these repulsive interactions these particles would flocculate as they reached their true equilibrium lowest energy state, the primary minimum. The CCA ordering will decrease if ionic impurities leach into the CCA. Further, the CCA must be sealed to avoid water evaporation. This is notoriously difficult to prevent since all organic materials have significant diffusion constants for water, and the optical devices must be contained in materials that transmit light. Further, the CCA transiently disorders due to mechanical shock.

The Asher group developed a much more rugged photonic crystal by embedding the CCA within a hydrogel matrix[10] (Figure 6.5). This was accomplished by UV photopolymerization of nonionic acrylamide and bisacrylamide derivatives and other crosslinkers and a UV photoinitiator that were added to the CCA. UV photopolymerization of these ~10 % acrylamide/bisacrylamide mixtures result in rugged polymerized CCA (PCCA) photonic crystals which are ~90 % water or other solvent. These PCCA are enabling photonic crystal structures, since they can be easily further processed to form more sophisticated functional photonic crystal materials.

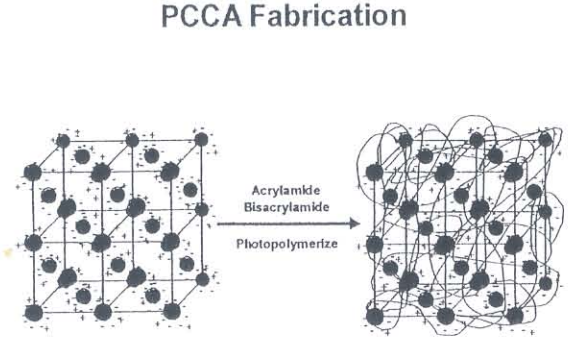

FIGURE 6.5. Synthesis of polymerized crystalline colloidal array (PCCA) by adding polymerizable monomers of acrylamide and bisacrylamide and a UV photoinitiator to a CCA. UV polymerization forms a hydrogel network around the CCA (~90 % water). The CCA crystal structure is maintained during polymerization and also upon hydrogel volume changes.

Another alternative to utilizing fragile CCA photonic crystals is to fabricate close-packed photonic crystals from monodisperse colloidal particles.[4,11] A number of groups have recently developed methods to grow highly ordered close packed arrays from solution dispersions of monodisperse particles. These methods rely on the controlled growth of particle layers on the growing crystal lattice surfaces. Additional processing of this lattice can form inverse opal structures. In this case, additional material is imbibed into the interstices between the close packed spheres. This material is then treated to remove the original close packed spheres,[11] leaving the material in the interstices between close packed arrays of air spheres.

6.2. DIFFRACTION FROM CCA PHOTONIC CRYSTALS

6.2.1. DIFFRACTION EFFICIENCIES AND BAND GAPS

The diffraction from CCA photonic crystals made from ~120 nm polystyrene spheres in water is extremely efficient. For example, Figure 6.6 shows a transmission measurement of an fcc colloidal crystal[9] which is oriented with the normal to the fcc (111) planes parallel to the incident light propagation direction. The diffraction of light at ~500 nm gives rise to a symmetric bandshape in the Figure 6.6 extinction spectra, which are scaled as -log of the transmission.

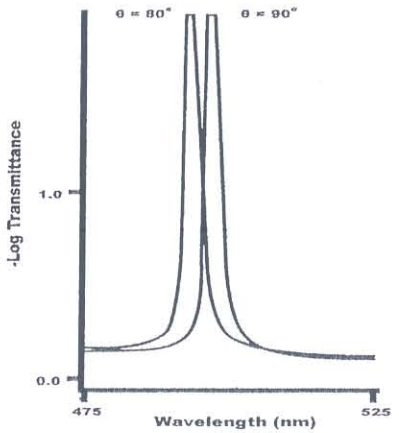

FIGURE 6.6. Extinction spectra of CCA of ~100 nm spheres. The diffraction band at ~500 nm shows a top hat profile since all incident light of a bandwidth of 5 nm is diffracted. The diffraction blue-shifts as the crystal is tilted to 80° off of the normal.

The simplest model for diffraction from these photonic crystals assumes the weak diffraction kinematic limit in which Bragg's law is operative: $\lambda_o \sim 2\, n\, d \sin\theta$, where λ_o is the wavelength of light in vacuum, n is the average refractive index of the photonic crystal, d is the spacing of the lattice planes diffracting and θ is the Bragg glancing angle. In this model, CCA with numerous layers give rise to insignificant small diffraction bandwidths.

In contrast, diffraction from CCA of polystyrene spheres in water shows significant bandwidths; essentially all light that meets the diffraction condition is diffracted from even thin CCA (Figure 6.6). The extinction spectrum (shown giving a top hat profile with a ~5 nm bandwidth blue-shifts as the CCA is tilted off of normal (almost following Bragg's law). The finite

bandwidth occurs because the polymer spheres in water show large scattering cross sections for visible light. Thus, efficient diffraction occurs; the incident beam traversing the sample is highly attenuated as the diffracted beam grows in intensity. This incident beam attenuation limits the number of layers involved in diffraction and determines the bandwidth of diffraction. The stronger the diffraction, the fewer layers involved in the scattering, and thus, the broader the diffraction.[12]

We initially modeled the diffraction from polymer colloid CCA by using Dynamical Diffraction theory[12] as did Spry and Kosan.[13] Dynamical diffraction theory predicts highly efficient diffraction and successfully explains the sphere diameter, and the angular and wavelength bandwidth diffraction dependence. As pointed out recently by Mittelman and Colvin et al,[14] more sophisticated theoretical approaches are needed to model the photonic crystal diffraction for particles with a higher refractive indices and for polystyrene sphere sizes above ~150 nm.

The efficiency of diffraction increases as the modulation depth, $M_D = [(m_s / m_i)^2 - 1]$ of the diffracting particles increases, where m_s and m_i are the refractive indices of the spheres and the material in the interstices between spheres, respectively. Even more sophisticated theoretical approaches are required for larger values of M_D where multiple scattering dominates.[1-5] It appears clear from photonic crystal theory that fabrication of a 3-D photonic bandgap crystal in the visible spectral region lies just at the edge of what is possible given known materials. For example, a 3-D photonic bandgap is predicted to just occur in an inverse fcc crystal (the interstices have the larger refractive index) if the refractive index of interstices is 2.8 and the spheres are etched out and have the refractive index of vacuum.

The lack of a 3-D bandgap in the direct fcc lattice results because the diffracting planes are unable to diffract π polarized incident light[15] when $\theta = 45°$. This leaves a small solid angle for this light to propagate. No other planes are situated to diffract this light. Apparently, the inverse opal fcc structure closes this gap for sufficiently large refractive index differences between the interstices and the spherical voids.

The theories that are used to model CCA diffraction and to predict diffraction bandwidth do not yet include phonons and Debye-Waller phenomena which are known to contribute to diffuse scattering. Our examination of these phenomena in the early 90's found that diffraction from even well ordered CCA shows significant diffuse scattering from these dynamic phenomena as well as from static disorder such as defects.[16] Recent theoretical studies suggest that existence of 3-D photon bandgap materials is highly sensitive to lattice defects structures.

Figure 6.7 shows the diffraction spectra of 270 nm polystyrene sphere CCA in water along well defined crystalline planes. An *apparent* 3-D

photonic bandgap appears at ~600 nm where little light transmission occurs at any orientation of the crystal in the incident beam. Transmission experiments were performed where the crystal orientation was scanned over all possible incident angles. These experiments showed that all light propagation directions appear to be effectively closed. This 3-D bandgap is likely to be due in part to phenomena such as diffuse scattering and defect scattering.

Thus, some features of a 3-D photonic bandgap material appears to occur even for periodic materials that do not meet the strict conditions required for the opening of a gap. These easily fabricated polystyrene colloid photonic crystals, with their relatively small refractive index differences can be utilized to demonstrate interesting optical phenomena.

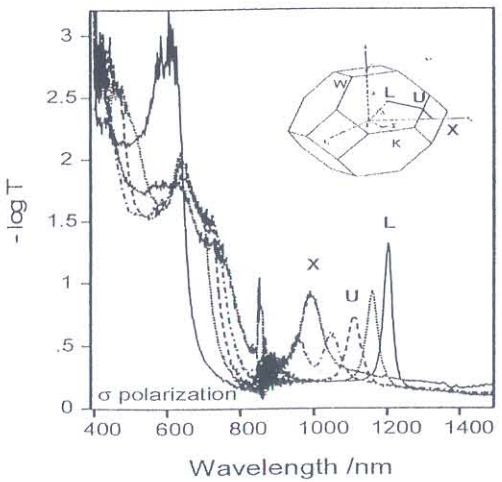

Figure 6.7. Extinction spectra of 125 μm thick CCA of 270 nm diameter polystyrene spheres in water recorded at different rotation angles within the L-U-X plane and with the incident light polarized perpendicular to the incident plane. The L direction corresponds to normal incidence, U is rotated by 35°, and X is rotated 55° from normal. As the sample is tilted, the (111) diffraction peak moves from ~1200 nm to ~1000 nm, where it is coincident with the (200) peak. The broad band at ~600 nm at normal incidence is a superposition of several peaks from the (200), (220), and (311) families of planes.

6.2.2. STANDING WAVE ELECTRIC FIELD LOCALIZATION

An important feature of photonic crystals is that they can be used to localize the electric field maxima of light within materials. This may be useful, for example, for increasing the nonlinear optical response of

materials. This electric field localization was recently demonstrated by Wang and Asher[18] in their study of the plasmon resonance extinction of a CCA of silver quantum dots contained within silica spheres. For example Figure 6.8 shows the concentration dependence of the CCA diffraction as well as the surface plasmon extinction of an aqueous CCA of 82 nm silica spheres containing Ag quantum dots. The dark curve in Figure 6.8 also shows for comparison the extinction of a random dispersion of these same spheres in a DMSO-water solution. All of the extinction spectra were normalized to the particle concentration of the random dispersion.

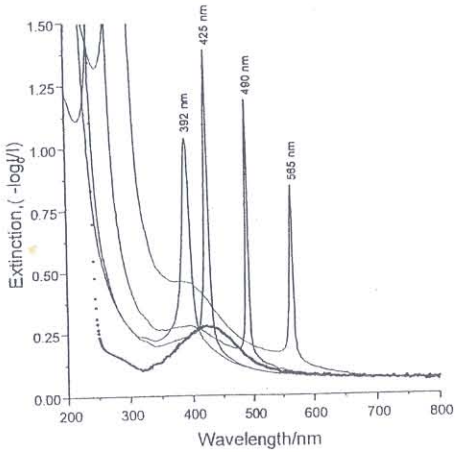

FIGURE 6.8. Comparison of extinction spectra of CCA of 82 nm diameter Ag@SiO_2 composite colloids at different particle concentrations (solid lines) to the extinction spectrum of a random dispersion of the particles in an n=1.47 water-DMSO refractive index matching solvent (heavy line). The extinction spectra are normalized to the particle concentration of the random refractive index matched dispersion (7.43 vol%).

The CCA fcc (111) plane spacing decreases as the sphere number density increases, which causes the diffraction band to blue-shift towards the plasmon absorption at ~430 nm. Surprisingly, the extinction spectrum showing the 425 nm diffraction peak displays a decreased plasmon absorption, much below that of the random dispersion. This clearly indicates that the transmitted light experiences a decreased plasmon resonance extinction.

Wang and Asher proposed that this decreased plasmon resonance extinction results from an analog of the Bormann effect observed in x-ray scattering, where the standing wave of the electromagnetic radiation in the periodic medium localizes the electric field in the low dielectric component (Figure 6.9), in the water in our case. This decreases the plasmon

absorption. In contrast, the diffraction on the blue side of the plasmon resonance localizes the electric field maxima in the high dielectric constant medium, giving rise to an increased plasmon absorption.

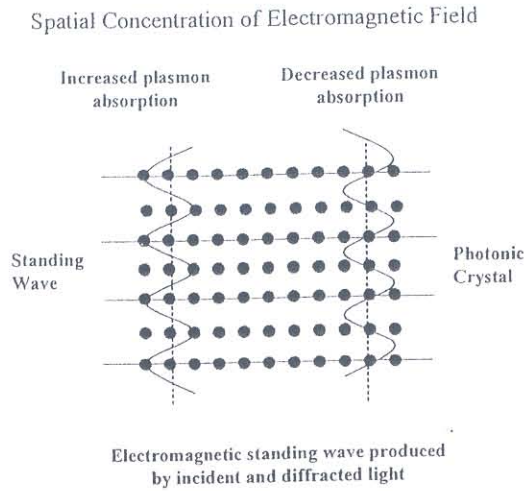

FIGURE 6.9. Schematic illustration of the Borrmann effect in a CCA photonic crystal. A standing wave is produced by the coupled incident and diffracted light. If the electric field maximum lies in the particle planes the absorption is a maximum, while if the electric field maximum lies between the particle planes, the absorption is a minimum.

This shows that the periodic spacing of a photonic crystal can be tuned to maximize the electric field within this periodic medium. This phenomenon has the potential to increase the nonlinear response of materials. In fact, it was recently used to increase the absorption of dyes on the red edge of the diffraction band. This was recently demonstrated by the Mallouk[19] group who showed a standing wave induced increased red edge absorption in a photonic crystal photovoltaic device that increased the solar photovoltaic efficiency by increasing the dye absorption bandwidth.

6.3. CCA OPTICAL SWITCHING AND OPTICAL LIMITING

The CCA diffraction can be altered by high intensity laser illumination.[20] Modest W/cm^2 laser fluences can heat absorbing CCA to induce temperature increases which induce a diffraction shifts. This phenomenon occurs because of the temperature dependence of the repulsive interactions between colloidal particles (Figure 6.10). The major impact of CCA heating, in the absence of photochemistry, is to decrease the value of ε, essentially the dielectric constant of water. This dielectric constant

determines the value of U(r) directly, as well as through κ, the reciprocal of the Debye length. A temperature increase decreases ε, which decreases the repulsion between spheres. This results in a local compression of the CCA by the surrounding colder CCA, which results in a local diffraction blueshift. An additional blue shift derives from the accompanying decrease in the average CCA refractive index.

This laser heating induced diffraction shift can be used for slow switching of transmission or diffraction from a CCA. However, attempts to speed up this process by faster heating, such as by pulsed laser sources disorder the CCA, probably due to shear forces induced by fluid motion. These liquid CCA may be too fragile for use in fast optical switching materials.

We also examined other CCA optical switching approaches. For example, we developed a synthesis for monodisperse, highly charged poly-N-isopropylacrylamide (NIPAM) colloidal particles.[21] These particles undergo a dramatic temperature dependent volume phase transition from a highly swollen polymer in water below room temperature, to a dramatically shrunken polymer above room temperature; the polymer shrinks by expelling water and becomes relatively hydrophobic. As shown in Figure 6.10A these spheres undergo a volume phase transition, where the diameter decreases from 300 nm to 100 nm as the temperature increases from 15 to 35 °C. The scattering power of the spheres, as measured by turbidity, increases dramatically for the shrunken spheres, because the sphere refractive index rapidly increases as the sphere volume decreases. These spheres readily self assemble into an fcc CCA which diffracts light in the visible spectral region. The diffraction of the fcc can be continuously controlled by controlling the CCA temperature. As shown in Figure 6.10 the CCA, which minimally diffracts 500 nm light at low temperature, diffracts essentially all of the incident 500 nm light at high temperature.

This CCA NIPAM volume phase transition phenomenon may be useful for fabricating optical switches or optical limiters. For example, optical limiting applications would utilize incident laser heating as the actuating temperature increase. Unfortunately, the switching times for these NIPAM CCA are slow (sec). Attempts to heat the sample quickly with pulsed or CW laser sources result in transient sample disorder. Presumably, the liquid CCA ordering is too fragile to permit fast switching.

6.4. POLYMERIZED COLLOIDAL ARRAY SWITCHING AND OPTICAL LIMITING

As discussed above we fabricated more robust photonic crystal materials by polymerizing acrylamide hydrogels around the CCA lattice of colloidal particles.[10] These polymerized CCA (PCCA) possess the responsive properties of hydrogels.

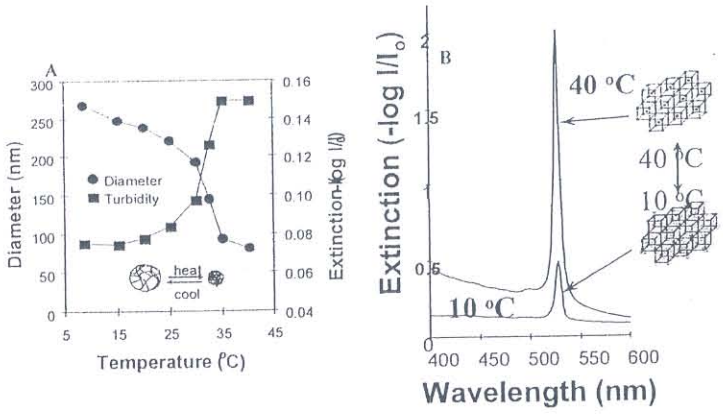

FIGURE 6.10. A: Dependence of diameter of monodisperse N-isopropylacrylamide colloids on temperature. The diameter was monitored by quasielastic light scattering. The temperature dependence of the turbidity of a random dispersion is also shown. B: Dependence of diffraction of a CCA of these colloidal particles at 10 and 40 °C.

Normal acrylamide hydrogels in water show little volume response to changes in temperature or aqueous solution ionic strength. However, large hydrogel volume changes can be induced by altering the surrounding hydrogel solvent composition which alters the free energy of mixing of the hydrogel with the solvent[22] A PCCA relative volume change of dV/V results in a relative CCA lattice spacing change and a relative diffraction wavelength change of $dl/l = d\lambda/\lambda \sim 1/3\ (dV/V)$, for small volume changes. Obviously, these hydrogel volume changes can be used to tune the PCCA diffraction wavelength.

These PCCA can also be chemically functionalized to make them responsive to temperature, photon flux and their chemical environment. This enables novel photonic switching materials which can be used for photonic control of diffraction and for fabricating chemical sensing photonic crystals.

6.4.1. PCCA THERMAL DIFFRACTION SWITCHING PHENOMENA

The kinetics of hydrogel volume phase transitions depends on the effective size of the hydrogel. ~100 μm thick hydrogels respond in time scales of seconds. The response is slow because any hydrogel volume change must macroscopically transport water into or out of the hydrogel. Theory[23] indicates that the response is diffusion-like in nature, and should scale as $t \sim l^2$. Thus, faster PCCA volume phase transitions require smaller hydrogel length scales. For example, if we utilize ~100 nm hydrogels we expect ~1 μsec time scales.

In fact, this expectation is met. Figure 6.11 shows the temperature dependence of diffraction from a PCCA array of NIPAM colloidal particles lightly polymerized into a PCCA hydrogel. After these NIPAM spheres self-assembled into a CCA lattice they were lightly polymerized into an acrylamide/bisacrylamide PCCA. This permanently localized the sphere centers of mass at the fcc lattice sites. As expected, the CCA diffraction efficiency dramatically increases as the temperature increase causes the NIPAM spheres to collapse (Figure 6.11). Because the centers of mass of the individual spheres are locked onto an fcc lattice, this array of NIPAM spheres does not disorder upon laser heating. In fact it shows very fast (μsec) optical switching.

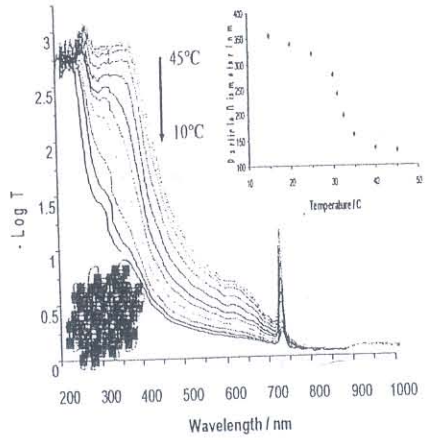

FIGURE 6.11. Temperature dependence of diffraction from PCCA of NIPAM spheres. The inset shows the temperature dependence of the diameter of the individual spheres in water. The diffraction efficiency increases with temperature as the sphere size decreases. The peak at ~730 nm results from diffraction by the fcc (111) plane. The shoulder at ~630 nm is from a higher Miller index plane and indicates that the fcc planes have buckled. Diffraction at shorter wavelengths derive from higher index planes and second order diffraction[17].

Figure 6.12 shows the time dependence of diffraction from the PCCA of NIPAM spheres subsequent to excitation by a 3 nsec pulse of 1.9 μm light that is absorbed by the surrounding H_2O/D_2O medium. This near IR light, is converted to heat in the psec time domain, to give rise to a ~ 10 °C T-jump. The diffraction efficiency increase shows a short 1 μsec time constant which accounts for 26 % of the diffraction increase, while the remaining efficiency increase derives from slower 20 μsec and 200 μsec dynamics. The 600 nm peak derives from diffraction from the fcc 111 planes while the diffraction at 300 nm derives from second order diffraction. The broad diffraction between 300 and 600 nm derives from diffraction from misaligned planes.

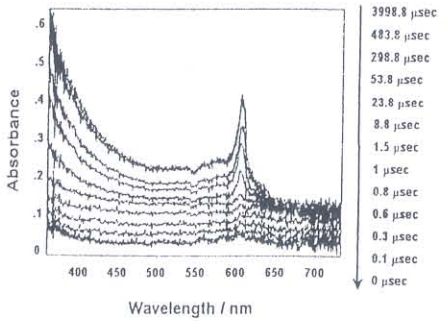

FIGURE 6.12. Time dependence of diffraction of PCCA of NIPAM spheres shown in Figure 6.11. The PCCA was excited by a 3 nsec 1.9 μm IR pulse which generates a ~10°C T-jump. A xenon flashlamp interrogates the transmission at different delay times. The transmission spectrum is monitored by a fiber optic diode array spectrometer.

Obviously, the use of ~100 nm spheres enables fast μsec optical switching times. In fact, we should be able to achieve even faster switching behavior by constructing photonic crystals out of even smaller particles.

6.4.2. PCCA PHOTOCHEMICAL SWITCHING PHENOMENA

We have also developed photochemically switchable PCCA[24] by covalently attaching azobenzene derivatives. The trans ground state of azobenzene in solution shows a strong near UV absorption band at ~360 nm (Figure 6.13). Monophotonic excitation within this absorption band converts the trans form to the cis form which displays a weak~460 nm absorption. The cis form shows a large activation barrier which prevents conversion back into the trans ground state, such that at room temperature in the dark,

the cis form PCCA is stable for more than one week. Population of the cis derivative red shifts the PCCA 710 nm fcc (111) diffraction band to 730 nm due to the cis derivative's increased dipole moment, which results in a more favorable free energy of mixing. This redshifted diffraction can be completely reset to 710 nm by excitation in the visible to convert the cis to the trans derivative. Because this PCCA is macroscopic, these photochemically induced diffraction shifts are slow and occur ~10 sec after 3 nsec UV or visible excitation. This PCCA response is obviously too slow for optical switching or optical limiting applications, but could be useful for memory devices. Excitation in the UV writes information in the form of redshifts in the diffraction which creates an image. Subsequent excitation in the visible erases the stored information. Readout occurs at wavelengths that do not cause diffraction shifts.

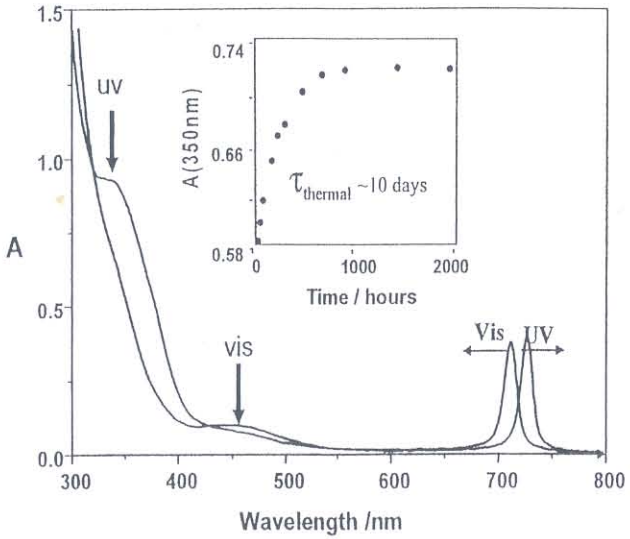

FIGURE 6.13. Optical switching of azobenzene functionalized PCCA. UV light transfers trans ground state azobenzene to the cis form while visible light transfers cis azobenzene to the trans form. The more favorable free energy mixing of the cis form results in a diffraction redshift of the fcc (111) diffraction from 710 to 730 nm. Inset shows that cis form is stable for ~10 d.

Interestingly, we also observe fast (300 nsec) diffraction shift dynamics in this system.[24] Excitation in the UV results in a prompt ~5 nm red-shift which relaxes back to the initial diffraction in ~1 msec time, and which evolves in the multisecond time scale to a stable cis red shifted diffraction. We are continuing to investigate these phenomena.

6.4.3. PCCA REFRACTIVE INDEX DIFFRACTION SWITCHING PHENOMENA

We are also developing a fast optical switching photonic crystal[25] where the PCCA colloidal particles have the real part of their refractive index matched to that of the medium (Figure 6.14). Thus, under normal circumstances the array does not diffract light. However, these colloidal particles also have an imaginary component of their refractive index which selectively absorbs incident laser irradiation.[26,27] The resulting particle temperature increase causes the particle refractive index to diverge from that of the medium. Thus, upon high laser fluences the array refractive index modulation "pops up" to diffract away in incident laser wavelength.[25]

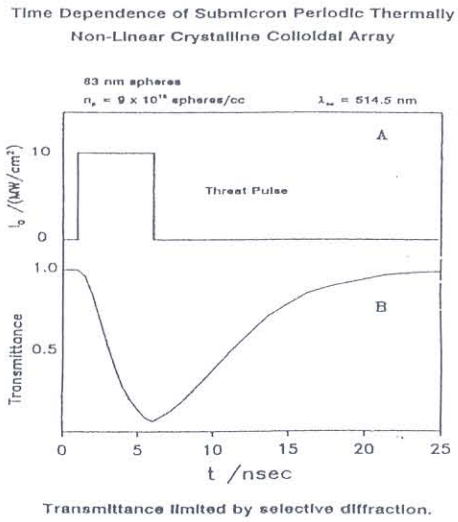

FIGURE 6.14. Concept for optical limiting involving absorbing colloidal particles (n_p) that are refractive index matched to the medium (n_m). At normal incident intensities the system transmits light except for a ~45 % attenuation by absorption[25]. High intensity illumination heats the spheres, lowers their refractive index and causes the CCA refractive index modulation to "pop up" to diffract away the incident light.

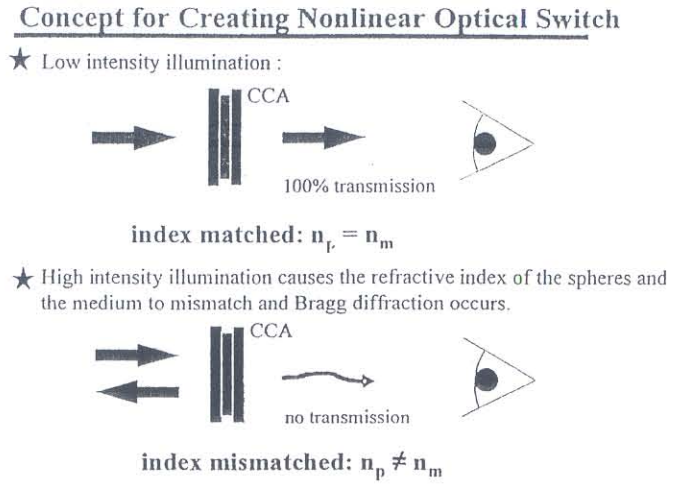

FIGURE 6.15. Calculated response[25] of CCA of absorbing 83 nm diameter spheres (9 X 10^{13} spheres/cm^3) which are initially refractive index matched to the medium. Excitation by a 5 nsec incident pulse with a fluence of 10 MW/cm^2 causes the array diffraction to "pop up" and to diffract away greater than 90 % of the incident light within within 6 nsec.

Most polymers show a temperature dependence of the refractive index, $dn/dT \sim -10^{-4}\ T^{-1}$. Thus, a temperature increase of 10 °C should decrease the PARTICLE refractive index by 0.001. This value of $\Delta n = n_p - n_m$ for a PCCA of ~100 nm diameter particles is calculated to be sufficient to diffract away most of the light meeting the Bragg condition.[25]

We also calculated[25] that we could use nsec pulsed lasers to selectively heat the PCCA colloidal particles, and this temperature increase would stay localized within the ~100 nm colloidal particles over nsec time intervals to selectively decrease the sphere refractive index compared to the medium.[25] A modeling of this system (Figure 6.15) indicated that optical limiting should occur in the ~5 nsec time scale for fluences of less than 10 MW/cm^2.

Experimental Setup For Measuring Optical Switching Nonlinearity

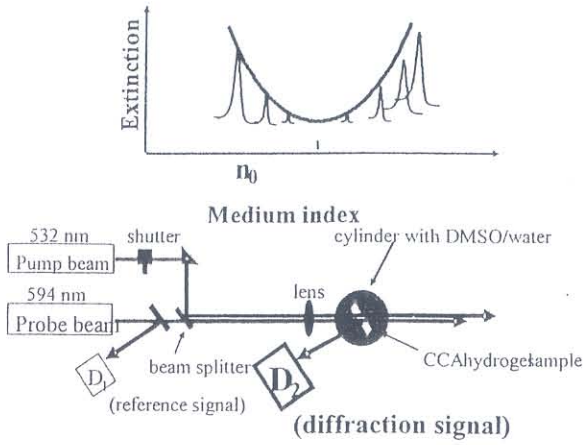

FIGURE 6.16. Top curve shows the dependence of diffraction on the refractive index difference between the particles and the medium. The diffracted intensity is zero when the refractive indices are equal and increases symmetrically with the absolute difference. Bottom: Experimental setup for monitoring diffraction from CCA shown in Figure 6.15. A 532 nm laser pulse (5 nsec duration) incident on the CCA heats the absorbing colloidal particles. A 594 nm delayed probe pulse is also generated by a dye laser excited by the 532 nm pulse. Two diodes monitor the relative intensity of the 594 nm probe pulse as well as the intensity diffracted by the CCA.

To test this switching mechanism we developed a synthesis of highly charged fluorinated colloidal particles containing absorbing dye.[26] These fluorinated particles have a refractive index of 1.38 and are easy to refractive index match to a mainly aqueous medium typical of PCCA.

We examined the optical switching by using a 3 nsec 532 nm pulsed laser which was absorbed by the PCCA colloidal particles.[25] We also utilized a 594 nm probe pulse which was diffracted by the heated CCA array (Figure 6.16).

As shown by Figure 6.17 we observe an increase in diffraction with increasing pump pulse energy when our colloidal particles have a refractive index below that of the medium ($n_p < n_m$). Larger pump pulse energies result in even smaller values of n_p, which increases the refractive index mismatch, which increases the diffraction. The dip at 0.6 mJ gives rise to a ~50 °C temperature increase to the polymer glass transition temperature. Higher pulse energies disrupt the PCCA ordering.

Figure 6.17 shows that the pump pulse does not alter the diffraction, if the spheres do not contain dye to absorb the light. Alternatively, if the dyed

colloidal particles have a refractive index greater than that of the medium, ($n_p > n_m$) pump heating decreases n_p which decreases the refractive index mismatch which decreases the diffraction efficiency.

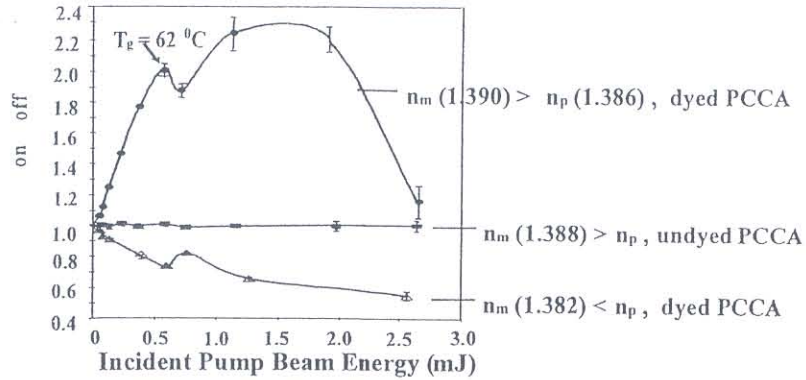

FIGURE 6.17. Pulse energy dependence of the relative diffraction (relative to that in the absence of the pump pulse) from the CCA of Figure 6.15. The middle curve is for undyed spheres that do not change refractive index. The top curve is for particles with a refractive index smaller than that of the medium, while the bottom curve is for particles with refractive index greater than that of the medium.

We examined the time dependence of these pump induced diffraction changes. Figure 6.18 shows that the maximum diffraction change is delayed by about 3 nsec from the pump pulse, as predicted.

Thus, we observe the predicted photonic crystal diffraction switching. Unfortunately, initial measurements only found 3 % diffraction switching efficiencies,[25] more recent studies have observed 7 % switching efficiencies. We are presently characterizing the phenomena that limit these efficiencies. These phenomena appear to be related to those contributing to the nsec diffraction peak shift dynamics observed for the azobenzene PCCA hydrogels briefly discussed above.

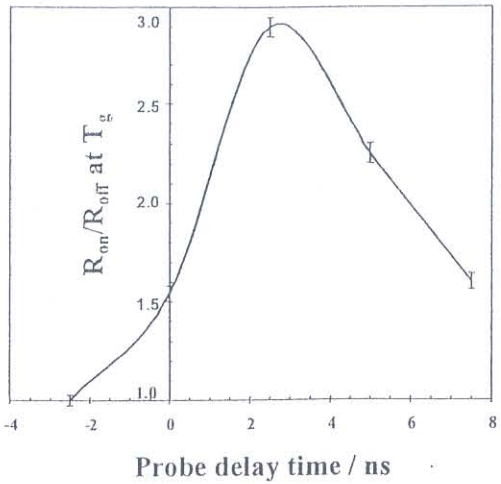

FIGURE 6.18. Probe delay time dependence of CCA diffraction. The maximum diffraction occurs at ~3 nsec after the pump pulse.

6.5. PCCA PHOTONIC CRYSTAL CHEMICAL SENSING MATERIALS

A crosslinked hydrogel is a responsive soft material whose volume is controlled by three competing phenomena,[22] the free energy of mixing of the hydrogel polymer with the medium, electrostatic interactions of charges bound to the hydrogel and the restoring forces due to the hydrogel crosslinks (Figure 6.19). The free energy of mixing of the hydrogel with the medium involves the entropic propensity of the hydrogel to fill all space (analogous to the entropy increase associated with the expansion of an ideal gas), and an enthalpic term which accounts for molecular interactions of the hydrogel with the medium.

The electrostatic free energy gives rise to osmotic pressures associated with electrostatic interactions between bound charges and osmotic pressures due to the changes in the water chemical potential associated with the immobilization of counterions within the hydrogel to the bound charges. Each charge immobilizes at least one counterion, to give rise to a hydrogel Donnan potential in low ionic strength solutions, which causes water to flow into or out of the hydrogel. Finally, the configurational entropy of the hydrogel crosslinked chains act to constrain the hydrogel volume.

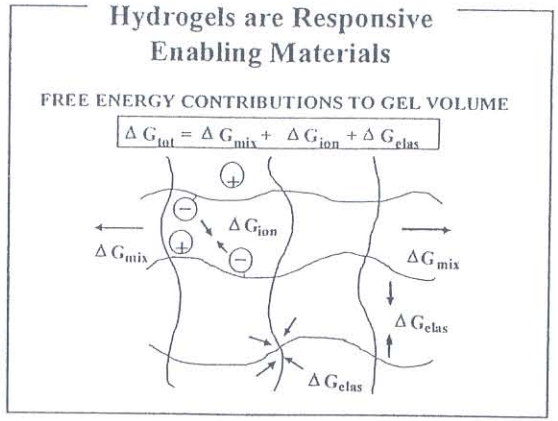

FIGURE 6.19. The hydrogel volume depends upon the free energy of mixing, the free energy of ionic interactions and the free energy associated with the elastic constraints of the hydrogel crosslinks.

We have functionalized[22] the PCCA with molecular recognition agents to create intelligent PCCA (IPCCA) which can be used for chemical and temperature sensing applications. These molecular recognition agents are designed to actuate PCCA hydrogel volume changes as they interact with their targeted analytes. These volume changes alter the embedded CCA lattice constants, which result in diffraction wavelength shifts which directly report on the concentration of analyte or temperature.

6.5.1. TEMPERATURE SENSING IPCCA SENSORS

The temperature sensors utilize the previously discussed volume phase transitions of NIPAM. We can fabricate a NIPAM PCCA temperature sensor by polymerizing a polystyrene colloid CCA in a NIPAM hydrogel.[21] Figure 6.20 shows that the temperature induced NIPAM volume phase transition shifts the diffraction from the near IR into the near UV as the PCCA temperature is varied between 15 and 40 °C. Thus, this PCCA material functions well as a highly sensitive temperature sensor.

The NIPAM volume phase transition, is driven by the temperature dependent free energy entropic term. The NIPAM hydrogel shrinks in order to minimize the surface area of hydrogel polymer contacting the water medium; water contacting the hydrophobic hydrogel must be highly ordered. The entropic penalty for this ordering of water at the polymer hydrogel interface increases linearly with temperature. At some temperature this becomes sufficiently unfavorable that it cannot be balanced by the expansion entropic free energy and the enthalpic term associated with the free energy

of mixing. This results in a shrinkage of the NIPAM hydrogel as it minimizes the surface area exposed to water.

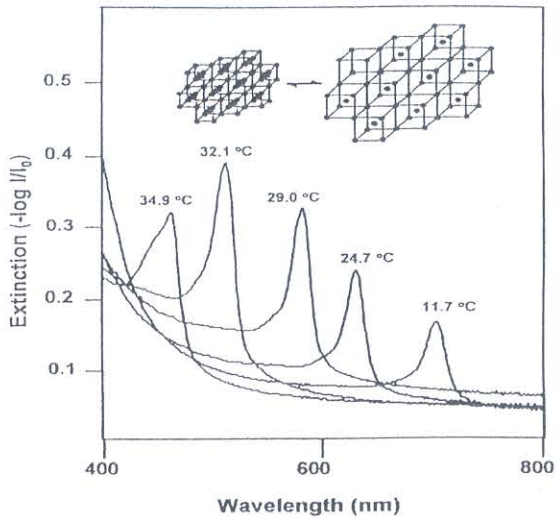

FIGURE 6.20. Temperature dependence of diffraction from a PCCA of polystyrene colloidal particles polymerized into a poly-N-isopropylacrylamide hydrogel. The diffraction shifts from ~720 nm at 12 °C to 460 nm at 34.9 °C. The diffraction shifts result from a volume phase transition due to free energy of mixing changes of the polymer with water as the temperature is altered.

6.5.2. ELECTROSTATICALLY DRIVEN CHEMICAL IPCCA SENSORS

Our first photonic crystal chemical sensors utilized a Donnan potential to drive the volume phase transition used for chemical sensing.[22] A vinyl-crown ether derivative with a high affinity for Pb^{2+} was polymerized into a PCCA (Figure 6.21). Ligation of the Pb^{2+} dication by the crown ether in the PCCA results in immobilization of its counterions, which causes a Donnan potential which induces an osmotic pressure which swells the hydrogel. nM to mM concentrations of Pb^{2+} are easily detected. The diffraction red shift reaches a maximum of ~650 nm and then decreases at concentrations above ~1000 ppm, due to the decreasing Donnan potential at the elevated solution ionic strengths that accompany the higher solution Pb^{2+} concentrations. This Pb^{2+} sensor can be immersed directly in the analyte solution to determine the analyte concentration by measuring the wavelength of light diffracted at normal incidence, for example. Alternatively, we demonstrated that this sensor material can be glued to the end of a fiber optic to determine the concentration remotely.[22]

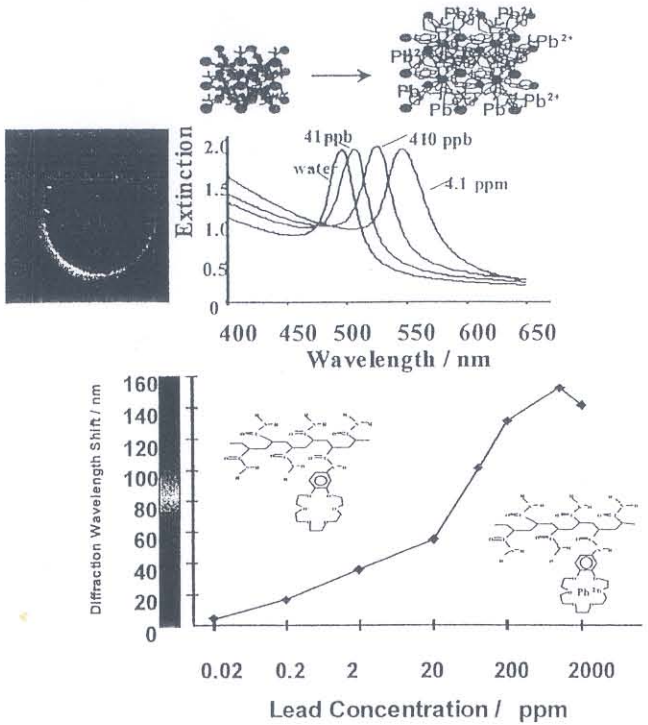

FIGURE 6.21. IPCCA containing 18-crown-6 recognition group has a high affinity for Pb^{2+}. Top left: photograph showing red (center) diffraction from originally blue (outer edges) IPCCA, after placing a drop of 8 mM $Pb(NO_3)_2$ on IPCCA. Dependence of diffraction peak and diffraction peak wavelength on Pb^{2+} concentration.

The selectivity's of these IPCCA sensing materials are determined by the selectivity's of their molecular recognition agents. Because this 18-crown-6 derivative[22] has a binding affinity for Ba^{2+} comparable to that for Pb^{2+}, Ba^{2+} is a significant interferant.

We fabricated a glucose sensing IPCCA by utilizing the enzyme glucose oxidase (GOD).[22] GOD converts glucose to gluconic acid. During this reaction a flavin is reduced in the enzyme. This anionic flavin acts as an anion immobilized on the hydrogel, which gives rise to a Donnan potential which swells the PCCA in proportion to the glucose concentration. This GOD PCCA operates as a steady-state sensor since oxygen in solution reoxidizes the flavin. When oxygen is excluded concentrations of glucose as low as 10^{-12} M are easily determined.[22]

We recently developed another glucose IPCCA sensor that also utilizes a Donnan potential by attaching boronic acid recognition groups to the PCCA.[28] Boronic acid derivatives are known to bind to the cis diols of

carbohydrates such as glucose. The binding of glucose to neutral boronic acid derivatives shifts the boronic acid equilibrium towards the anionic boronate form. This anionic boronate attached to the hydrogel results in a Donnnan potential induced osmotic pressure which swells the PCCA. As shown in Figure 6.22, this IPCCA is an excellent glucose sensor in low ionic strength aqueous solutions. The solid line through the diffraction shift data derives from a detailed hydrogel volume phase transition model which accurately models the IPCCA response.

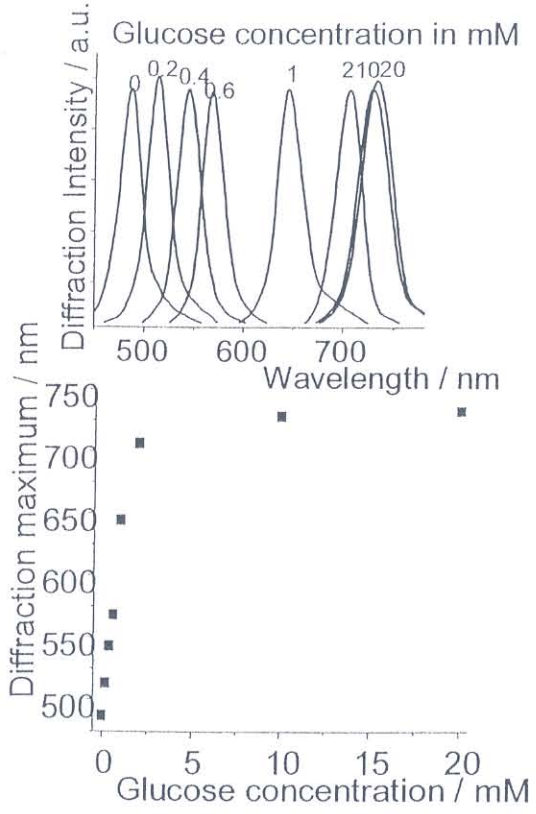

FIGURE 6.22. Glucose concentration dependence of diffraction from boronic acid IPCCA. The IPCCA in pure water redshifts as the glucose concentration increases until ~5 mM glucose concentration where the response saturates.

We also developed pH and ionic strength sensors which also utilized the hydrogel Donnan potential.[29] The pH sensor utilizes a covalently attached group which titrates in the pH range of interest. For example, to sense pH values between 4 to 8 we utilized carboxyl groups formed by the hydrolysis of the amide groups of the polyacrylamide PCCA. As the pH

changes the fraction of protonated carboxlys change and the hydrogel changes its volume. This IPCCA can determine solution ionic strengths if used at pH values where significant carboxylates exist, because the Donnan potential decreases with solution ionic strength.

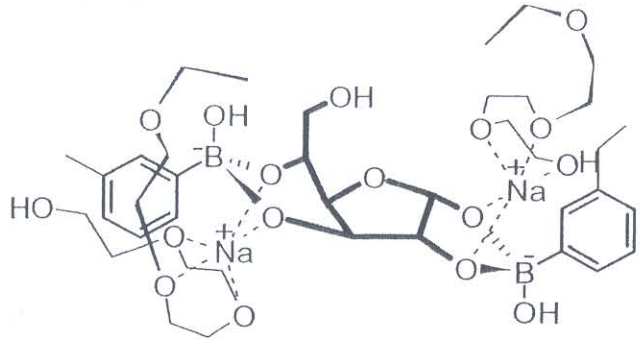

FIGURE 6.23. Model of glucose crosslinks across two boronates in IPCCA. The polyethylene glycol localizes two Na^+ cations at the boronates to reduce electrostatic repulsion between them.

6.5.3. CROSSLINKING DRIVEN IPCCA CHEMICAL SENSORS

We have also developed a sensor for glucose for use in high ionic strength bodily fluids based on glucose induced hydrogel crosslinking.[30] This sensor, which also utilizes boronic acids, also incorpororates polyethylene glycols. This IPCCA senses glucose through the crosslinks glucose forms through its two appropriately oriented cis diols (Figure 6.23). The formation of these crosslinks shrink the hydrogel as shown in Figure 6.24 for glucose concentrations between 0 and 10 mM glucose (the physiological ranges of glucose in tear fluids and blood) which blue shift the diffraction. Higher glucose concentrations break the crosslinks when individual glucose molecules saturate the individual boronic acid groups. We are now also able to fully model this sensor response using our fundamental understanding of the hydrogel volume phase transitions and the relationship between crosslinks and the IPCCA elastic constant. Our intention is to utilize these sensors for the noninvasive monitoring of glucose in the tear fluid of patients with diabetes mellitus.

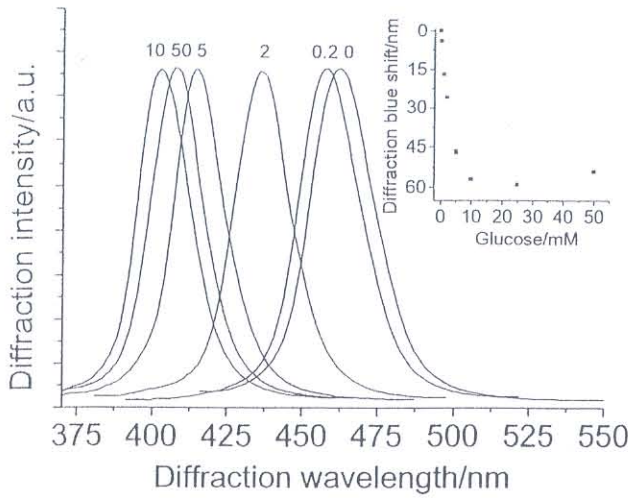

FIGURE 6.24. Glucose concentration dependence of diffraction of the 4-amino-3-fluorophenylboronic acid BA-AA-PEG sensor in 2 mM tris-HCl (pH 7.4) and 150 mM NaCl. Inset: Dependence of diffraction peak shift on glucose concentration.

6.6. CONCLUSIONS

As discussed above we are able to construct novel responsive photonic crystal materials which have promise for optical switching as well as chemical sensing devices. These materials interact with light due to their highly ordered CCA array. The prospects for these materials looks very bright to us.

ACKNOWLEDGEMENTS

We gratefully acknowledge financial support from NIH grant DK55348 and ONR grant N00014-94-1-0592 and Darpa grant DAAD16-99-C-1036.

REFERENCES

1. Joannopoulos, J.D.; Meade, R.D.; Winn, J.N. "*Photonic Crystals:Molding the Flow of Light*"Princeton University Press, New York, **1995**.
2. (a) Ibanescu, M.; Fink, Y.; Fan, S.; Thomas, E.L.; Joannopoulos, J.D. *Science* **2000**, *289*, 415; (b) Maldovan, M.; Urbas, A.M.; Yufa, N. W.; Carter, C.; Thomas, E.L. *Phys. Rev. B.* **2002**, *65*, 165123; (c) Soukoulis, C. M. Nanotechnology. **2002**, *13*, 420-423.

3. Sakoda,K. "*Optical Properties of Photonic Crystals*", Springer Series in Optical Sciences **2001**.
4. (a)Krauss , T. F.; De La Rue, R. M. .*Prog. Quant. Elect.* **1999**,*23*, 51-96; (b) Ozin , G. A.; Yang, S. M. *Adv. Func. Mat.* **2001**,*11*, 95-104.(c) Jiang, P.; Ostojic, G. N.; Narat, R.; Mittleman, D.V.; Colvin, L. *Adv. Mat.* **2001**, *13*, 389-393.(d) Norris, D. J.; Vlasov, Y. A. *Adv. Mat.* **2001**, *13*, 371-376.
5. (a) Busch, K.; John, S. *Phys. Rev. E.* **1998**, *58*, 3896-3908 .(b) Biswas, R. M.; Sigalas, M.; Subramania, G.; Soukoulis , C. M.; Ho, K. M. *Phys. Rev. B.* **2000**, *61*, 4549-4553.
6. (a) Carlson, R. J.; Asher, S. A. *Appl. Spectrosc.* **1984**, *38*, 297-304.(b) Flaugh, P. L.; O'Donnell, S. E.; Asher, S. A. *Appl. Spectrosc.* **1984**, *38*, 847-850 .(c) Asher, S. A. *U.S. Patent.* **1986**, # 4,627,689, # 4,632,517.(d) Asher, S. A.; Flaugh, P. L.; Washinger, G. *Spectroscopy* . **1996**, *1*, 26-31.
7. (a)Alfrey, T. Jr.; Bradford, E. B.; Vanderhoff, J. W.; *J. Opt. Soc. Am.* **1954** *44*, 603-609; (b) Krieger, I.M.; O'Neill, F. M. *J. Am. Chem. Soc.* **1968**,*90*, 3114.
8. (a)Hiltner, P. A.; Krieger, I. M. *J. Phys. Chem.* **1969**, *73*, 2386. (b) Hiltner, P. A.; Papir, Y. S., Krieger, I. M. J. *Phys. Chem.* **1971**, *75*, 1881.
9. Flaugh, P. L.; O'Donnell, S.; EAsher, S. A. *Appl. Spectrosc.* **1984**, *38*, 847-850.
10. (a)Asher, S. A.; Holtz, J.; Liu L.; Wu, Z. *J. Am. Chem. Soc.* **1994**, 4997-4999 (b) Asher, S. A.; S. Jagannathan, S. U.S. Patent # 5, **1994**, 281,370.(c) Haacke, G.;Panzer, H. P; Magliocco, L. G.; Asher, S.A. U.S. Patents # 5, **1993**, 266,238. #5,368,781 1994.
11. (a) Park, S. H.; Xia, Y. *Chem. Mat.* **1998**, 10, 1745; (b) Gates, B.; Qin, D.; Xia, Y. *Adv. Mat.* **1999**, 11, 466; (c) Zakhidov, A.; Baughman, R. H.; Iqbal, Z.; Cui, C.; Khayrullin, I.; Dantras, S.; Marti, J.; Ralchenko, V. G. *Science* **1998**, 282, 897; (d) Wijnhoven, J. E. G.; Vos, W. L. *Science* **1998**, 281, 802; (e) von Blaaderen, A.; Rue, R.; Wiltzius, P. *Nature* **1997**, 385, 241; (f) Jiang, P. ; Bertone, J. F.; Hwang, K. S.; Colvin, V. L. *Chem. Mater.* **1999**, 11, 2132.
12. Rundquist, P. A.; Photinos, P.; Jagannathan, S.; Asher, S. A. *J. Chem. Phys.* **1989**, 91, 4932-4941.
13. Spry, R. J.; Kosan, D. J. *Appl. Spectrosc.* **1986**, 40, 782.
14. Mittleman, D. M.; Bertone, J. F.; Jiang, P.; Hwang, K. S.; Colvin, V. L. *J. Chem. Phys.* **1999**, 111, 345.
15. Pan, G.; Sood, A. K.; Asher, S. A. *J. Appl. Phys.* **1998**, 84, 83-86.
16. (a)Rundquist, P. A.; Kesavamoorthy, R.; Jagannathan, S.; Asher, S. A. *J. Chem. Phys.* **1991**, 95, 1249-1257; (b) Rundquist, P. A.; Kesavamoorthy, R. ; Jagannathan, S.; Asher, S. A. *J. Chem. Phys.* **1991**, 95, 8546-8551.
17. Liu, L.; Li, P.; Asher, S. A. *J. Am. Chem. Soc.* **1997**, 119, 2729-2732.
18. Wang, W.; Asher, S. A. *J. Am. Chem. Soc.* **2001**, 123, 12528-12535.
19. Mallouk, T.; et al. *J. Am. Chem. Soc.* In press 2003.
20. (a) Rundquist, P. A.; Jagannathan, S.; Kesavamoorthy, R.; Brnardic, C.; Xu, S.; Asher, S.A. *J. Chem. Phys.* **1991**, 94, 711-717; (b) Kesavamoorthy, R.; Jagannathan, S.; Rundquist, P. A.; Asher, S. A. *J. Chem. Phys.* **1991**, 94, 5172-5179.
21. Weissman, J. M.; Sunkara, H. B.; Tse , A. S.; Asher, S. A. *Science* **1996**, 274, 959-960.

22. (a) Holtz, J. H.; Asher, S. A. *Nature.* **1997,** 389, 829-832; (b) Holtz, J. H.; Holtz, J. S. W.; Munro, C. H.; Asher, S. A. *Anal. Chem.* **1998,** 70, 780-791.
23. (a) Tanaka, T.; Hocker, L. O.; Benedek, G.B. *J. Chem. Phys.* **1973,** 69, 5151; (b) Tanaka, T.; Filmore, D. J. *J. Chem. Phys.* **1979,** 70, 1214; (c) Peters, A.; Candau, S. J. *Macromolecules.* **1986,** 19, 1952; (d) A. Peters and S.J. Candau, *Macromolecules.* 21, 2278 **1988**; (e) Li, Y.; Tanaka, T. *J. Chem. Phys.* **1990,** 92, 1365; (f) Annaka, M.; Tanaka, T. *Nature.* **1992,** 355, 430; (g) Durning, C. J.; Mormon, Jr., K. N. *J. Chem. Phys.* **1993,** 98, 4275; (h) Tokita, M.; Miyamoto, K.; Komai, T. *J. Chem. Phys.* **2000,** 113,1647.
24. Reese, C.; Mikonin, A.; Asher, S. A. *Adv. Func. Mat.* **2003,** *Submitted.*
25. Kesavamoorthy, R.; Super, M. S.; Asher, S. A. *J. Appl. Phys.* **1992,** 71, 1116-1123.
26. (a) Asher, S. A.; Kesavamoorthy, R.; Jagannathan, S.; Rundquist, P. *SPIE Vol. 1626 Nonlinear Optics III,* **1992,** 238-241; (b) Pan, G.; Kesavamoorthy, R.; Asher, S. A. *Phys. Rev. Lett.* **1997,** 78, 3860-3863; (c) Pan, G.; Tse, A. S.; Kesavamoorthy, R.; Asher, S. A. *J. Am. Chem. Soc.* **1998,** 120, 6518-6524; (d) Pan, G.; Kesavamoorthy, R.; Asher, S. A. *J. Am. Chem. Soc.* **1998,** 120, 6525-6530.
27. Tse, A.; Wu, Z.; Asher, S. A. *Macromolecules* **1995,** 28, 6533-6538.
28. Asher, S. A.; Alexeev, V. L.; Goponenko, A. V.; Sharma, A. C.; Lednev, I. K.; Wilcox, C. S.; Finegold, D. N. *J. Am Chem. Soc.* **2003,** 125, 3322-3329.
29. Lee, K.; Asher, S. A. *J. Am. Chem. Soc.* **2000,** 122, 9534-9537.
30. Alexeev, V. L.; Sharma, A. C.; Goponenko, A.V.; Das, S.; Lednev, I. K.; Wilcox, C. S.; Finegold, D. N.; Asher, S. A. *Anal. Chem,* **2003,** 75, 2316-2323.

7

PLASMONIC NANOMATERIALS

Enhanced Optical Properties From Metal Nanoparticles and their Ensembles

Alexander Wei
Department of Chemistry, Purdue University

7.1. INTRODUCTION

The first examples of nanotechnology, some historians might be inclined to argue, could very well be accredited to some glassblowers from the days of imperial Rome. Those ancient craftsmen were able to embed colloidal metal particles within their glassy works to enhance their lustrous qualities. Although they were most likely unaware of the nanoscopic nature of these inclusions, this did not prevent them from appreciating the enigmatic hues produced upon a change of incident light. One of the most striking examples of such Roman glasses is the famed Lycurgus cup, which dates back to the 4th century A.D. The chalice has a dark greenish tint under reflected lighting, but when illuminated from behind the goblet appears red colors are attributed to the optical responses of colloidal gold particles dispersed throughout the glass. Similar phenomena are also featured in the stained-glass windows of many medieval cathedrals, most often from colloidal particles of coinage metals such as copper and gold (red) or silver (yellow).